Stimulus repetition modulates gamma-band synchronization in primate visual cortex

Nicolas M. Brunet[a,b,1], Conrado A. Bosman[a,c,1], Martin Vinck[d,1], Mark Roberts[a,e], Robert Oostenveld[a], Robert Desimone[f], Peter De Weerd[a,e], and Pascal Fries[a,d,2]

[a]Donders Institute for Brain, Cognition, and Behaviour, Radboud University Nijmegen, 6525 EN Nijmegen, The Netherlands; [b]Department of Neurological Surgery, University of Pittsburgh, Pittsburgh, PA 15213; [c]Cognitive and Systems Neuroscience Group, Swammerdam Institute for Life Sciences, Center for Neuroscience, University of Amsterdam, 1098 XH Amsterdam, The Netherlands; [d]Ernst Strüngmann Institute (ESI) for Neuroscience in Cooperation with Max Planck Society, 60528 Frankfurt, Germany; [e]Department of Cognitive Neuroscience, Faculty of Psychology and Neuroscience, Maastricht University, 6200 MD Maastricht, The Netherlands; and [f]McGovern Institute for Brain Research, Massachusetts Institute of Technology, Cambridge, MA 02139

Edited by Ranulfo Romo, Universidad Nacional Autonóma de México, Mexico City, Mexico, and approved January 20, 2014 (received for review May 23, 2013)

When a sensory stimulus repeats, neuronal firing rate and functional MRI blood oxygen level-dependent responses typically decline, yet perception and behavioral performance either stay constant or improve. An additional aspect of neuronal activity is neuronal synchronization, which can enhance the impact of neurons onto their postsynaptic targets independent of neuronal firing rates. We show that stimulus repetition leads to profound changes of neuronal gamma-band (~40–90 Hz) synchronization. Electrocorticographic recordings in two awake macaque monkeys demonstrated that repeated presentations of a visual grating stimulus resulted in a steady increase of visually induced gamma-band activity in area V1, gamma-band synchronization between areas V1 and V4, and gamma-band activity in area V4. Microelectrode recordings in area V4 of two additional monkeys under the same stimulation conditions allowed a direct comparison of firing rates and gamma-band synchronization strengths for multiunit activity (MUA), as well as for isolated single units, sorted into putative pyramidal cells and putative interneurons. MUA and putative interneurons showed repetition-related decreases in firing rate, yet increases in gamma-band synchronization. Putative pyramidal cells showed no repetition-related firing rate change, but a decrease in gamma-band synchronization for weakly stimulus-driven units and constant gamma-band synchronization for strongly driven units. We propose that the repetition-related changes in gamma-band synchronization maintain the interareal stimulus signaling and sharpen the stimulus representation by gamma-synchronized pyramidal cell spikes.

adaptation | learning | oscillation | plasticity | priming

Stimulus repetition typically leads to reduced neuronal firing rates and reduced functional MRI blood oxygen level-dependent signals, whereas behavior that is based on stimulus processing is not affected or is enhanced (1). Different models have been proposed to reconcile these behavioral and neurophysiological findings (1). In a "fatigue model," neuronal responses are reduced in proportion to their amplitude, leaving relative response patterns unchanged; in a "sharpening model," neurons that code features irrelevant to identification of a stimulus exhibit repetition suppression, leading to a sparser and sharpened representation of the repeated stimulus; and in a "facilitation model," stimulus repetition leads to faster stimulus processing, and thereby smaller overall neuronal activity. Gotts and coworkers (2–4) suggested a "synchronization model" in which stimulus repetition leads to reduced firing rates accompanied by increased synchronization. The increased synchronization might explain how less-activated neuronal groups can maintain their impact onto postsynaptic neurons and, ultimately, behavior, while reducing metabolic costs at the same time. The synchronization model has received support from a number of studies in human subjects, using source-localized magnetoencephalography. Ghuman et al. (5) report enhanced frontotemporal 14-Hz synchronization for repeated vs. novel stimuli. Gilbert et al. (3) found that stimulus repetition leads to enhanced 5- to 15-Hz power in the right fusiform gyrus and enhanced 15- to 35-Hz power in striate and extrastriate cortex. Corresponding data were also reported for multisite microelectrodes recordings in striate and parietal cortex of awake cats, where von Stein et al. (6) found that interareal alpha-band synchronization was stronger for repeated compared with novel stimuli. The common finding across these studies is enhanced alpha/beta activity or coupling for repeated stimuli. The alpha coupling reported by von Stein et al. (6) occurs in a behavioral context and has a phase relationship and layer specificity that suggests a top-down–directed interaction. Thus, enhanced alpha/beta activity or coupling for repeated stimuli might reflect enhanced top-down signaling, perhaps related to enhanced predictability of repeated stimuli. However, increased synchronization with stimulus repetition according to the model of Gotts and coworkers (2–4) should also serve the maintenance of feedforward signaling of repeated stimuli in the face of reduced firing rates. Feedforward signaling has been strongly linked to local and interareal gamma-band synchronization (7–9). Local gamma-band synchronization likely enhances the postsynaptic impact of the precisely synchronized output spikes (10). Interareal gamma-band synchronization likely aligns excitability cycles such that inputs arrive when postsynaptic target neurons are receptive (11, 12). However, whether multiple presentations of a stimulus result

Significance

When a visual stimulus repeats multiple times, visual cortical neurons show decreasing firing rate responses, yet neither perception nor stimulus-related behavior is compromised. We show that stimulus repetition leads to increased neuronal gamma-band (~40–90 Hz) synchronization within and between early and higher visual areas. The enhanced gamma-band synchronization likely maintains effective stimulus signaling in the face of dwindling firing rates. We also show that synchronization to the gamma rhythm increases for spikes in general and for those of putative interneurons, whereas it decreases for spikes of putative excitatory neurons if they are not strongly stimulus-driven. Thus, inhibitory interneurons might create increasingly precise gamma-band synchronization, and thereby prune the stimulus representation by pyramidal cells to be sparser and more efficient.

Author contributions: N.M.B., C.A.B., M.R., R.O., R.D., P.D.W., and P.F. designed research; N.M.B., C.A.B., and P.F. performed research; N.M.B., M.V., and P.F. analyzed data; and N.M.B. and P.F. wrote the paper.

The authors declare no conflict of interest.

This article is a PNAS Direct Submission.

Freely available online through the PNAS open access option.

[1]N.M.B., C.A.B., and M.V. contributed equally to this work.

[2]To whom correspondence should be addressed. E-mail: pascal.fries@esi-frankfurt.de.

This article contains supporting information online at www.pnas.org/lookup/suppl/doi:10.1073/pnas.1309714111/-/DCSupplemental.

in enhanced gamma-band synchronization remains unknown (details are provided in *SI Discussion*). We investigated gamma-band synchronization within and between macaque monkey areas V1 and V4 and report that stimulus repetition leads to profound changes in gamma-band synchronization within and between these areas.

Results

We investigated repetition-related changes in gamma-band synchronization in two datasets, each containing data from two awake macaque monkeys (details of stimulus, task, and recording are provided in *Methods*). The first dataset was obtained from two monkeys (monkeys E1 and E2) implanted with an electrocorticographic (ECoG) grid covering many superficial areas, including areas V1 and V4. The second dataset was obtained from two monkeys (monkeys M1 and M2) and was recorded with standard tungsten microelectrodes in area V4. For both datasets, monkeys were fixating while one or two eccentric patches of drifting grating were presented and the monkeys monitored either the fixation point or one of the grating patches.

Stimulus Repetition Leads to Increasing Area V1 Gamma-Band Activity. We sorted trials according to trial number into eight equally sized and nonoverlapping trial bins. For each trial bin, Fig. 1*A* shows a representative raw local field potential (LFP) trace. Traces are from one recording site in area V1 from one recording session in monkey E1. Fig. 1*B* shows the trial bin averages of the absolute and baseline-normalized power spectra and demonstrates that repeated presentations resulted in increasing gamma-band responses. Fig. 1*C* shows the gamma power as a function of trial bin number. Visually induced gamma-band (52–74 Hz) power was highly correlated to the logarithm of the trial bin number (r^2 = 0.98, P = 4.0e-06). Fig. S1 shows the same analysis as in Fig. 1*B* (*Inset*), but averaged over all sites with significant visually driven gamma-band activity and averaged over three sessions. During these recording sessions, the monkey reported color changes of the fixation point, and the peripheral grating stimulus, which induced gamma-band activity, was behaviorally irrelevant. This suggests that the repetition-related gamma increase did not depend on attention being directed to the gamma-inducing stimulus. Gamma-band activity in these sessions was particularly strong because a full-field grating was used (13).

For the following analyses, we will use data from recording sessions during which the monkeys performed a selective visual attention task with grating patches of 3° of visual angle. If not otherwise stated, we use data from the task period when the stimuli were on the screen and attention had been deployed to one of them, and we pool across the two selective attention conditions. Fig. 1*D* depicts the spatial distribution of all ECoG electrodes on the brain of monkey E1, and Fig. 1*E* shows the visually induced gamma-band power change (stimulation vs. baseline, 52–74 Hz) for all ECoG sites. Fig. 1*F* shows the power spectra averaged over the significantly visually driven area V1 sites of monkey E1 for eight nonoverlapping trial bins (62 of a total of 63 sites; details are provided in *Methods*), averaged further across 25 sessions (6,266 trials). Fig. 1*I* shows the average gamma-band power and the corresponding SE across sessions. When the trial bin number was expressed on a logarithmic scale, there was a near-perfect log-linear relation to the gamma increase (r^2 = 0.99, P = 1e-07). Next, we investigated the spatial

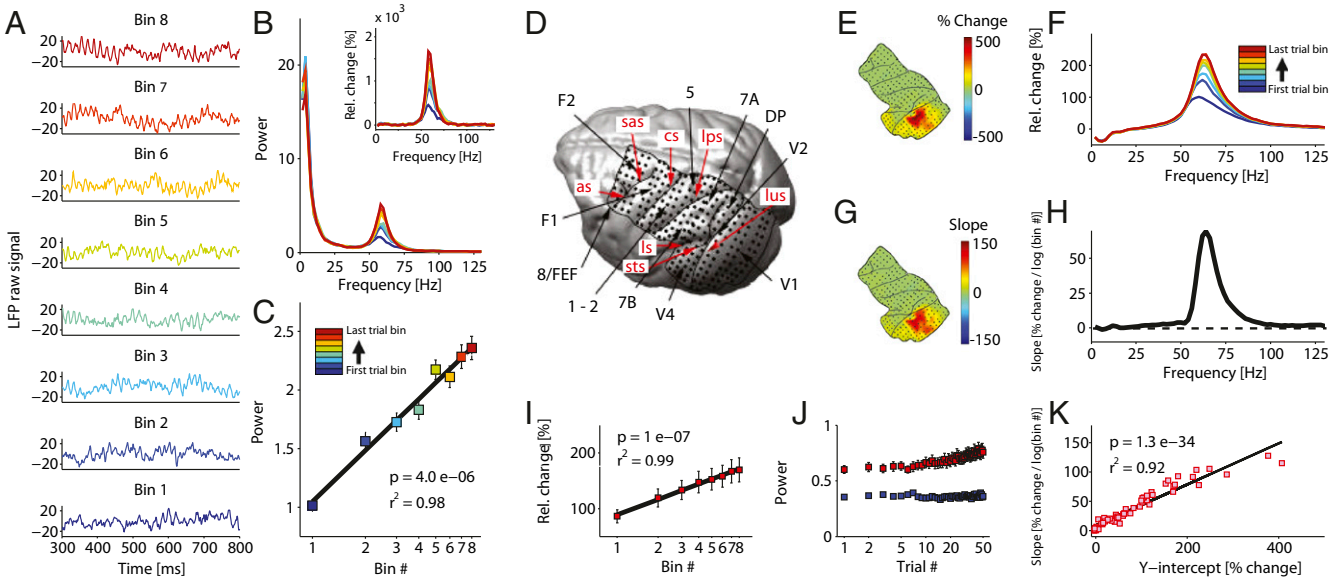

Fig. 1. Stimulus repetition enhances gamma-band activity in visual cortex. (*A*) Raw LFP traces from one representative recording site from area V1 and eight representative trials from one recording session in monkey E1. During this session, monkey E1 performed a color change detection at fixation and the gamma-inducing grating stimulus was behaviorally irrelevant. (*B*) Corresponding absolute and baseline-normalized power spectra. Rel., relative. (*C*) Gamma power as a function of trial bin number on a logarithmic scale. Trials were sorted according to trial number into eight equally sized and nonoverlapping bins, and power was averaged per bin. (*D*) Brain of monkey E1 with ECoG electrodes and major sulci (as, arcuate sulcus; cs, central sulcus; ips, intraparietal sulcus; ls, lateral sulcus; lus, lunate sulcus; sas, spur of the arcuate sulcus; sts, superior temporal sulcus). Black labels point to the covered brain areas. (*E*–*K*) Data from sessions during which monkey E1 performed a selective attention paradigm. (*E*) Relative change in gamma power during stimulation compared with baseline, averaged over all trials. (*F*) Same as in *B* (*Inset*), but averaged over all visually driven area V1 sites and all sessions in monkey E1. Slopes of regression analyses are shown as in *I*, but separately for each site (*G*) and frequency (*H*). (*I*) Same as in *C*, but averaged over area V1 sites and sessions. (*J*) Trial-wise average of gamma-band power for the first 50 trials. Red squares show power during stimulation, and blue squares show power during baseline. (*K*) Each dot corresponds to a visually driven area V1 site in monkey E1. For each site, the regression analysis was performed separately and the scatter plot shows the respective slopes as a function of the intercepts. The intercept estimates the visually induced gamma-band power before the repetition-related increase occurred. This repetition-independent estimate of the stimulus-induced gamma-power change was predictive of the later repetition-related increase. Dots in *D*, *E*, and *G* show electrode positions, yet power estimates are based on sites (i.e., local derivatives). Absolute power values are shown in arbitrary units (a.u.) in *B*, *C*, and *J*.

and spectral specificity of the gamma increase. Fig. 1*G* color-codes the slope of regression lines that were obtained as shown in Fig. 1*I*, but separately for all ECoG sites. The topography of slopes (Fig. 1*G*) was very similar to the topography of visually induced gamma (Fig. 1*E*). This suggests that the increase was specifically related to visually induced activity rather than to drifts in the overall state of the brain or in the recording system. However, Fig. 1*E* shows the visually induced gamma-band activity averaged across all trials (i.e., including later trials in which the visually induced gamma-band activity was already affected by the repetition-related gamma increase). To avoid any circularity and to demonstrate the fine-grained dependence of the repetition-related gamma increase over trials on the visually induced gamma increase within trials, we performed the following analysis. For each of the sites showing clear visually induced gamma, we performed a separate regression analysis and extrapolated the regression line to the *y*-axis intercept for bin number zero, so as to use this intercept as an estimate of the visually induced gamma before any repetition-related increase occurred. We then investigated whether this intercept value predicted the repetition-related regression slope, by calculating a regression between the two parameters. Fig. 1*K* demonstrates a strong correlation (r^2 = 0.92, P = 1.3e-34), confirming that the repetition-related increase was systematically related to the strength of visually induced gamma-band activity. To investigate the spectral specificity of the increase, Fig. 1*H* shows the slopes for the visually driven sites, now as a function of frequency. The slope spectrum demonstrates that the repetition-related increase was specific for the gamma-frequency band, with a spectral shape very similar to the stimulus-induced gamma-power enhancements.

To test whether there was any stimulus-induced gamma-band power in the first few trials of a session, we averaged gamma-band power across sessions separately for each of the first 50 trials (Fig. 1*J*; red squares indicate absolute power during visual stimulation, and blue squares indicate absolute power during prestimulus baseline). This revealed that gamma-band activity was induced already by the very first stimulus presentation of a given session. This analysis also demonstrated that the increase was present for the absolute gamma-band power during visual stimulation (P = 2.8e-20 for monkey E1 and P = 3.5e-11 for monkey E2) and not for the absolute gamma-band power during prestimulus baseline (P = 0.98 for monkey E1 and P = 0.11 for monkey E2). This illustrates that the repetition effect on visually induced gamma power was not due to decreases in prestimulus, but rather to increases in poststimulus gamma-band power. Fig. S2 shows the same analysis for monkey E2, demonstrating a remarkable consistency across the two animals. In monkey E2, 39 area V1 sites were significantly stimulus-driven (of a total of 40 sites), nine recording sessions had been obtained (3,511 trials), and the gamma-frequency band extended from 68 to 82 Hz.

The fact that gamma increased with stimulus repetition both when the stimulus was a large unattended grating and when it was a smaller attended grating suggested that the effect did not depend on attention. We performed an additional analysis in this regard by analyzing the period when visual stimuli were already on the screen but no attentional cue had been given yet. Consistent with the other results, this showed the repetition-related gamma increase (Fig. S3). We also considered that the repetition-related increase was modulated by switches in stimulus features or in the allocation of attention. The respective analyses (Fig. S4) revealed only that the repetition-related increase was slightly larger for repetitions that involved a change in stimulus color, an effect that might be related to predictive coding (14).

Stimulus Repetition Leads to Increasing Area V1–V4 Gamma Coherence and Area V4 Gamma Activity. Gamma power in one area might contribute to communication with connected areas through interareal coherence (7, 8, 11, 12, 15, 16). Therefore, we tested whether the increase was also present for the coherence between area V1 and area V4. All analyses were done after bipolar derivation, thereby excluding a common reference, which can otherwise lead to artifactual coherence estimates. Fig. 2*A* (*Inset*) shows the anatomical definition of area V1 (pink) and area V4 (blue) in monkey E1 (*Methods*). Fig. 2*A* shows the interareal coherence for the eight trial bins averaged over all sessions in this monkey, revealing that interareal coherence also increased monotonically with trial number (62 significantly stimulus-driven area V1 sites of a total of 63 sites and 16 significantly stimulus-driven area V4 sites of a total of 17 sites, 992 interareal site pairs, and 6,266 trials). We performed the same regression analysis as for power, and we plot the resulting slope spectrum in Fig. 2*B*. The dominant result was a coherence increase in the gamma-frequency band. In addition, there was a smaller decrease in a theta-frequency band.

Enhanced gamma coherence between areas V1 and V4 is expected to result in enhanced gamma power in area V4 (12). Fig. 2*C* shows LFP power spectra from area V4 of monkey E1 (16 significantly stimulus-driven sites of a total of 17 sites and 6,266 trials), and Fig. 2*D* shows the corresponding slope spectra, confirming a repetition-related increase in area V4 power in the gamma-frequency band. Fig. S5 shows the repetition-related changes in area V1–V4 coherence and area V4 power for monkey E2, demonstrating that the gamma increase was consistent across the two animals (39 significantly stimulus-driven area V1 sites of a total of 40 sites, 16 significantly stimulus-driven area V4 sites of a total of 17 sites, 624 site pairs, and 3,511 trials).

We considered that the increases in local and long-range gamma-band synchronization could be related to changes in behavior. Therefore, we analyzed behavioral parameters in the same way as power and coherence, by binning trials and performing a regression analysis. This did not reveal any significant effect for response accuracy, for reaction times, or for the rate of microsaccades.

Stimulus Repetition Leads to Increases in the Gamma-Peak Frequency. Recent studies have shown that not only the strength but also the frequency of gamma-band activity can change systematically (e.g., with contrast) (8, 17). Correspondingly, we investigated the gamma

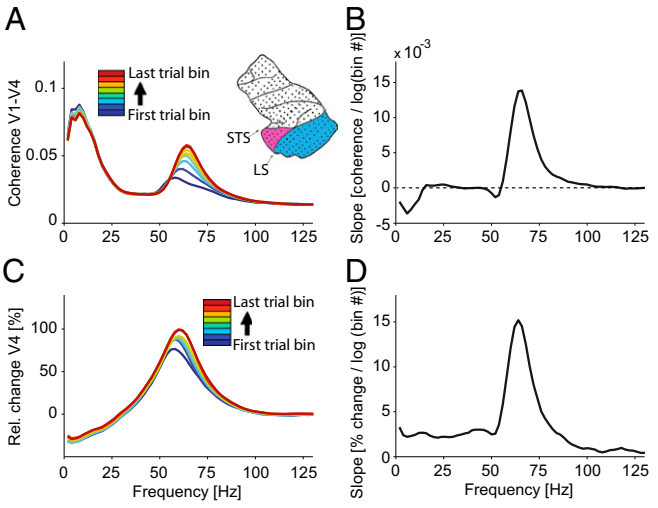

Fig. 2. Stimulus repetition enhances gamma-band coherence between areas V1 and V4 and the gamma-band power in area V4. (*A*) Coherence spectra for monkey E1, averaged over 25 recording sessions and all possible pairs of interareal sites. (*Inset*) Monkey E1 areas V1 (blue) and V4 (pink). LS, lunate sulcus; STS, superior temporal sulcus. (*B*) Slope of the regression of coherence vs. log(trial bin number) as a function of frequency. (*C* and *D*) Same as in *A* and *B*, but for V4 power.

frequency. Fig. S6 shows that for area V1 power, area V1–V4 coherence, and area V4 power, stimulus repetition makes the center of mass of the gamma band move to higher frequencies. This holds for both monkeys.

Stimulus Repetition Leads to Increasing MUA-LFP Synchronization in Area V4. Next, we investigated whether the increases in area V1 gamma power, area V1–V4 gamma coherence, and area V4 gamma power were also reflected in the gamma-band spike-LFP synchronization in area V4. To this end, we analyzed another dataset (monkeys M1 and M2) in which single-unit activity (SUA), multiunit activity (MUA), and LFPs were recorded from four electrodes simultaneously in awake monkey area V4, with electrodes spaced horizontally by 650 or 900 μm. Fig. 3 shows the effects of stimulus repetition on a sample MUA recording and its MUA-LFP synchronization. Fig. 3*A* shows that the firing rate of this MUA declined substantially over the course of 600 stimulus repetitions. Fig. 3 *B* and *C* illustrates that at the same time, the MUA synchronization to the LFP gamma rhythm increased. This is quantified in Fig. 3*D* by the pairwise phase consistency (PPC) between MUA (recorded on one electrode) and the LFP (combined across the other electrodes). The PPC is a recently introduced synchronization metric (18, 19) that avoids any bias by trial number, spike number, or spike rate (details are provided in *Methods*). To avoid strong nonstationarities, the first 0.3 s after stimulus onset was excluded. Fig. 4*A* shows the MUA-LFP PPC using the same data epoch as Fig. 3*D* and the same trial-binning approach as for power and interareal coherence, averaged across all MUA-LFP pairs of both monkeys. Averaging over both monkeys was possible because their gamma-frequency bands were largely overlapping (40–60 Hz) (20). Stimulus repetition led to a clear increase in gamma-band MUA-LFP synchronization, which was highly significant in the regression analysis (Fig. 4*B*; $r^2 = 0.91$, $P = 2.5\text{e-}04$; $n = 109$). Fig. 4*C* shows the regression slopes as a function of frequency and demonstrates that the increase was selectively present in the gamma-frequency band, whereas a low theta band showed a decrease. Fig. S7 demonstrates that this result was consistent across the two monkeys. Enhanced gamma-band MUA-LFP synchronization does not necessarily entail enhanced MUA rates (21), and previous demonstrations of repetition-related firing rate decreases in inferotemporal cortex (22–24) suggest that similar decreases might occur in area V4. Fig. 4*D* shows the normalized MUA rates (±1 SEM) averaged across all sites and sessions in both monkeys M1 and M2. There was a highly significant decrease of MUA firing rates with increasing trial number ($r^2 = 0.94$, $P = 8.2\text{e-}05$).

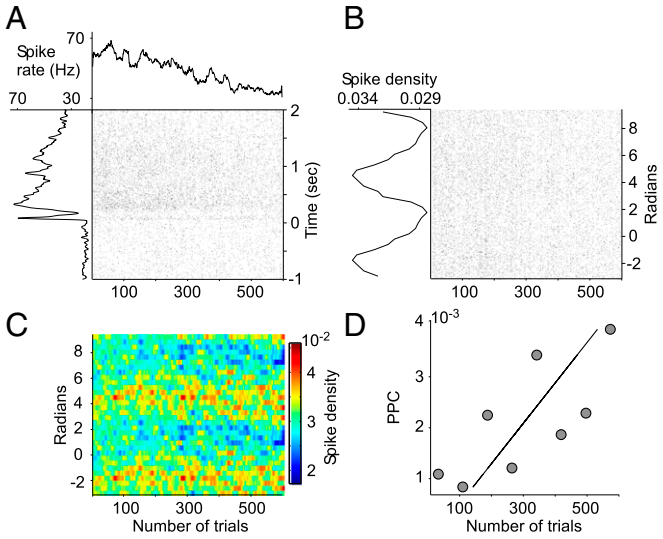

Fig. 3. Evolution of firing rate and spike-LFP phase synchronization for a sample multiunit response. (*A*) Spike rate as a function of time relative to stimulus onset (*Left*) and as a function of trial number (*Upper*, moving average across 15 subsequent trials). (*Right*) Spike rasters of single trials, with each dot corresponding to a spike. Note that we show poststimulus time up to 2 s after stimulus onset, yet target or distracter changes and corresponding trial ending could occur before that. If a trial ended earlier than 2 s after stimulus onset, the remaining time of that trial is discarded. (*B*, *Left*) Spike density (a.u.) as a function of LFP gamma (50 Hz) phase. Spike density was computed using a histogram with 16 bins and then ensuring that the densities plotted sum to 1. (*B*, *Right*) Spike rasters of single trials, with each dot corresponding to a spike. All spikes of a given trial (from 0.3 s poststimulus onset until one of the stimuli changed) are displayed in the corresponding column, irrespective of trial length and resulting number of gamma cycles. As a result, longer trials lead to stronger filling of the column with spikes. *A* and *B* are provided at high resolution in Fig. S9. (*C*) Spike density as a function of LFP gamma (50 Hz) phase, calculated as a moving average across 15 subsequent trials. (*D*) Gamma-band (50 Hz) spike-LFP PPC values for eight nonoverlapping trial bins. The x value of each dot indicates the mean trial number of the respective bin.

Stimulus Repetition Modifies Spike-LFP Synchronization in a Cell Class-Specific Way. In area V4, single units could be sorted, based on their waveforms, into narrow-spiking (NS) cells, which are putative interneurons, and broad-spiking (BS) cells, which are putative pyramidal cells (25, 26). We performed such a differentiation and analyzed firing rates and gamma-band synchronization separately for the two cell groups. Fig. 4*E* shows the average waveforms and the waveform duration histogram for the available single units, sorted into NS cells (red) and BS cells (blue). Fig. 4*F* shows the SUA-LFP PPC in the gamma-frequency band (difference relative to the first trial bin) separately for NS and BS cells: Gamma synchronization increased for the NS cells ($r^2 = 0.8$, $P = 0.003$; $n = 16$) and showed a strong tendency to decrease for the BS cells ($r^2 = 0.5$, $P = 0.05$; $n = 26$). Fig. 4*G* shows the corresponding spike rates; interestingly, the firing rates of NS cells decreased ($r^2 = 0.55$, $P = 0.035$), whereas there was no significant change in BS cell firing rates.

To reconcile the decreasing BS cell gamma synchronization with the increasing MUA gamma synchronization, we reasoned that weakly active and/or weakly stimulus-driven BS cells, which contribute fewer spikes to the MUA, might show strong decreases in synchronization, whereas strongly active and/or strongly driven BS cells, which contribute more spikes to the MUA, might show fewer decreases or even increases in synchronization. To test this hypothesis, we calculated a multiple linear regression between the firing rate and the regression slope. Concretely, we defined the independent firing rate (FR) variables [$FR_{baseline}$] and [$FR_{stimulation}/FR_{baseline}$] and the dependent variable [slope of the regression between synchronization strength and log (repetition bin number)]. Fig. 4*H* shows in blue the *t* values of this multiple linear regression for the BS cells. The dark blue line is for the independent variable [$FR_{stimulation}/FR_{baseline}$] and reveals that, indeed, when a BS cell was more strongly stimulus-driven, it showed a more positive slope of the repetition-related gamma change ($P = 0.0042$). The same analysis for the NS cells (Fig. 4*H*, red lines) did not reveal significant effects. To follow up the result for the BS cells, we performed a median split based on the stimulus-driven firing rate change and averaged the PPC vs. repetition slopes separately for the two groups of cells. This revealed a significant negative slope for the weakly driven BS cells ($P = 0.015$; mean slope ± SEM = −0.0028 ± 0.001) and an absence of a significant repetition-related change for the strongly driven BS cells ($P = 0.9$; mean slope ± SEM = 0.0001 ± 0.0001). We also sorted the BS cells into those with a decreasing slope ($n = 15$; three cells were individually significant) and those with an increasing slope ($n = 11$; one cell was individually significant).

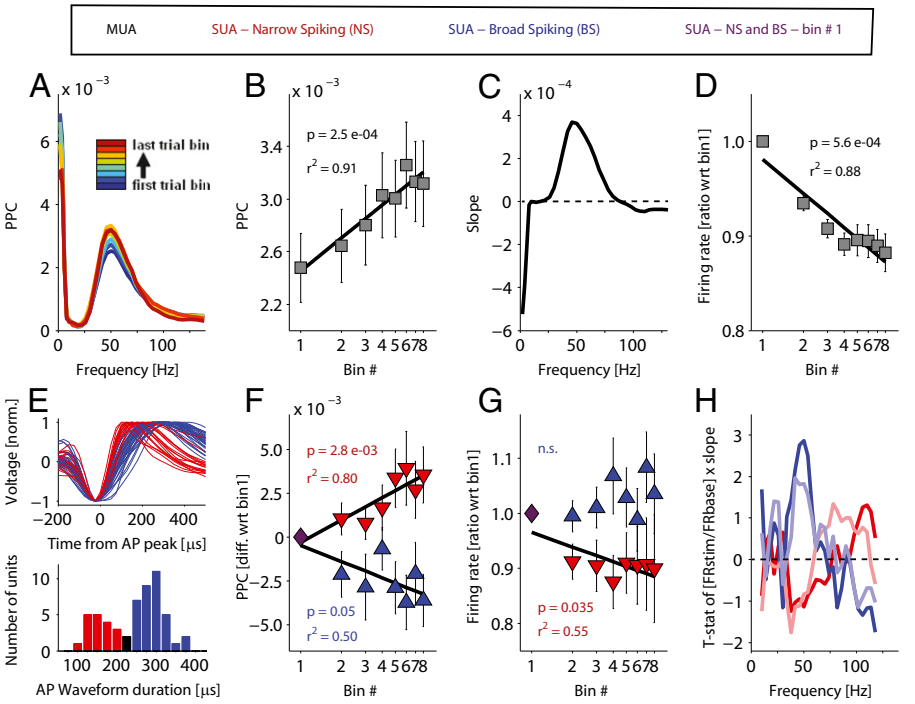

Fig. 4. Effect of stimulus repetition on the gamma-band spike-LFP synchronization. (*A*) PPC of multiunit spikes with regard to the spectral phase of the LFP recorded on neighboring electrodes (details are provided in *Methods*). (*B*) PPC from *A* as a function of trial bin number. (*C*) Slopes of regression analyses as shown in *B*, as a function of frequency. (*D*) Ratio of MUA firing rate with regard to the first trial bin, as a function of trial bin number, and the corresponding regression analysis. (*E*) Spike waveforms (averages per isolated single unit) and the distribution of the corresponding action potential waveform durations. Neurons with waveform durations in the black bin were discarded. norm., normal. (*F*) Change in PPC with regard to the first trial bin (diff. wrt bin 1), separately for NS and BS cells. (*G*) Ratio of the firing rate with regard to the first trial bin (ratio wrt. bin 1), separately for NS and BS cells. (*H*) Regression *t* statistics from two separate multiple linear regression analyses for the BS and NS cells, respectively. The multiple linear regressions fitted the dependent variable [slope of the regression between spike-LFP PPC and log(trial bin number)] as a function of the independent variables (firing rate in the baseline), with results shown as softly colored lines, and [firing rate during stimulation (FRstim)/firing rate in the baseline (FRbase)] NS (BS) waveforms. All panels show grand averages of all microelectrode recordings (i.e., averages across monkeys M1 and M2, across all recordings sessions, and across all sites or units, respectively). All recording sites were in area V4.

The index $[(FR_{stimulation} - FR_{baseline})/(FR_{stimulation} + FR_{baseline})]$ was, on average, 0.23 ± 0.12 for BS cells with negative slope and 0.49 ± 0.11 for BS cells with positive slope (difference not significant).

Discussion

We found that in the course of a recording session, during repeated stimulus presentations, gamma-band activity in area V1 increased by approximately a factor of 2. The strength of gamma-band activity was linearly related to the logarithm of the repetition bin number. This repetition-related gamma increase was spatially specific for the sites with visually induced gamma, and the strength of the repetition-related increase was systematically related to the strength of the visually induced gamma before any repetition-related increase. Furthermore, the repetition-related gamma increase did not appear to be dependent on selective visual attention. A very similar repetition-related increase was also present for the interareal gamma-band coherence between areas V1 and V4 and for the gamma-band activity in area V4. In a separate dataset from area V4, we showed that multiunit synchronization to the gamma rhythm increased by roughly 30%, whereas the multiunit rate decreased by roughly 12%. When separating single units into BS and NS cells, the NS cells showed qualitatively the same synchronization and rate changes as the multiunit. The BS cells showed a strong trend for a repetition-related decrease in gamma synchronization, which was significant for the weakly stimulus-driven cells but absent for the strongly driven ones.

Repetition-related increases in area V1 gamma-band activity and area V1–V4 gamma-band synchronization are expected to lead to an increasing impact of area V1 input onto area V4 (7, 11, 12). Because this increasing impact is rhythmic in the gamma-frequency band, it is expected to result, in area V4, in increasing gamma-band activity and increasing gamma spike-field synchronization but not necessarily in increasing overall firing rates, in line with the results reported here. It is conceivable that the overall firing rate decrease in area V4 is related to the increased gamma-rhythmic impact and the increased local gamma spike-field synchronization. We have shown previously that spikes that are maximally synchronized to the local gamma rhythm are more stimulus-selective than less gamma-synchronized spikes (27). With repeating stimulation, increasing area V1–V4 coherence, and corresponding impact, the less gamma-synchronized spikes in area V4 seem to disappear, leaving the more gamma-synchronized spikes from the more stimulus-driven neurons (Fig. 4*H*). The precise mechanisms of this pruning of non–gamma-synchronized spikes are unclear. They might well be a consequence of the increasing gamma-band synchronization, or they might be independent of the mechanisms behind gamma and its repetition-related increase.

From a methodological point of view, the present results are important for the interpretation of previous studies and for the optimal design of future studies on gamma-band synchronization. Typically, neurophysiological studies use multiple repetitions of a given experimental condition. Where previous studies confounded their experimental conditions with repetitions (e.g., by presenting conditions in blocks of trials without sufficient counterbalancing), this might have resulted in apparent condition effects that actually were repetition effects. Where previous studies properly randomized conditions across repetitions, the repetition-related effect described here might have led to an underestimation of the significance and/or size of the effect of the respective experimental conditions. For future studies on gamma-band synchronization, the present results emphasize the importance of proper condition randomization in the experiment design and of taking repetitions into account in the data analysis. A discussion of related studies (22–24, 28–36) is provided in *SI Discussion* and Fig. S8.

In Fig. 4, we analyzed the changes in gamma synchronization separately for MUA, NS cells, and BS cells. NS cells are putative interneurons, although this cannot be proven in the awake monkey preparation at this moment. Networks of interneurons are the core generators of gamma-band synchronization (26, 37). Consistent with this, the gamma synchronization of the NS cells

increased similar to the gamma power/coherence within/between ECoG signals. Intriguingly, the BS cells showed repetition-related changes in gamma synchronization that depended on their stimulus-driven activation. Weakly driven BS cells showed repetition-related decreases in gamma synchronization, whereas strongly driven BS cells kept their gamma synchronization unchanged across repetitions. Thus, across repetitions, the gamma-synchronized spike output contained fewer and fewer spikes from weakly stimulus-driven BS cells and relatively more spikes from strongly stimulus-driven BS cells, which amounts to a sharpening of the stimulus representation in the gamma-synchronized spike output (27). We have recently described a very similar effect of selective attention on cell type-specific gamma-band synchronization (26). It is particularly the gamma-synchronized spikes that have an impact on postsynaptic target neurons, and in this postsynaptic target group of neurons, the different input neurons always mutually reduce impact through normalization mechanisms (38). Thus, if the gamma-synchronized spike output contains relatively more spikes from strongly stimulus-driven BS cells, this lends those cells a stronger effective impact.

Methods

A detailed description of the methods used in this study is provided in *SI Methods*. If not stated otherwise, data are from recording sessions in which the monkeys performed a selective visual attention task. They kept fixation on a central dot while two patches of drifting grating were presented, of which one fell into the receptive field of the recorded neurons. In monkeys E1 and E2, ECoG grid electrodes were implanted over the left hemisphere to obtain LFPs (7, 39, 40). We use electrodes over areas V1, V2, and V4 and the temporal-occipital area (TEO). When we refer to area V1 (V4), this also includes some electrodes that might be over area V2 (TEO). LFPs from immediately neighboring electrodes were subtracted to obtain local bipolar derivations, which avoid a common reference in interareal coherence analysis. In monkeys M1 and M2, standard techniques were used to record with four microelectrodes simultaneously in visual area V4 (20, 41).

ACKNOWLEDGMENTS. We thank Edward Chang for help with implanting monkey E2, Paul Gaalman for help with structural MRI recordings, and Wolf Singer and Alina Peter for helpful comments to earlier versions of this manuscript. This work was supported by Human Frontier Science Program Organization Grant RGP0070/2003 (to P.F.); Volkswagen Foundation Grant I/79876 (to P.F.); the European Science Foundation's European Young Investigator Award Program (to P.F.); a European Union HEALTH-F2-2008-200728 Grant (to P.F.); the Landes-Offensive zur Entwicklung Wissenschaftlich-ökonomischer Exzellenz program grant "Neuronale Koordination Forschungsschwerpunkt Frankfurt" (to P.F.); the Smart Mix Programme of the Netherlands Ministry of Economic Affairs and the Netherlands Ministry of Education, Culture, and Science (BrainGain) (P.F. and R.O.); and The Netherlands Organization for Scientific Research Grant 452-03-344 (to P.F.).

1. Grill-Spector K, Henson R, Martin A (2006) Repetition and the brain: Neural models of stimulus-specific effects. *Trends Cogn Sci* 10(1):14–23.
2. Gotts SJ (2003) *Mechanisms Underlying Enhanced Processing Efficiency in Neural Systems* (Carnegie Mellon University, Pittsburgh).
3. Gilbert JR, Gotts SJ, Carver FW, Martin A (2010) Object repetition leads to local increases in the temporal coordination of neural responses. *Front Human Neurosci* 4:30.
4. Gotts SJ, Chow CC, Martin A (2012) Repetition Priming and Repetition Suppression: A Case for Enhanced Efficiency Through Neural Synchronization. *Cogn Neurosci* 3(3-4): 227–237.
5. Ghuman AS, Bar M, Dobbins IG, Schnyer DM (2008) The effects of priming on frontal-temporal communication. *Proc Natl Acad Sci USA* 105(24):8405–8409.
6. von Stein A, Chiang C, König P (2000) Top-down processing mediated by interareal synchronization. *Proc Natl Acad Sci USA* 97(26):14748–14753.
7. Bosman CA, et al. (2012) Attentional stimulus selection through selective synchronization between monkey visual areas. *Neuron* 75(5):875–888.
8. Roberts MJ, et al. (2013) Robust gamma coherence between macaque V1 and V2 by dynamic frequency matching. *Neuron* 78(3):523–536.
9. Buffalo EA, Fries P, Landman R, Buschman TJ, Desimone R (2011) Laminar differences in gamma and alpha coherence in the ventral stream. *Proc Natl Acad Sci USA* 108(27): 11262–11267.
10. Azouz R, Gray CM (2003) Adaptive coincidence detection and dynamic gain control in visual cortical neurons in vivo. *Neuron* 37(3):513–523.
11. Fries P (2005) A mechanism for cognitive dynamics: Neuronal communication through neuronal coherence. *Trends Cogn Sci* 9(10):474–480.
12. Womelsdorf T, et al. (2007) Modulation of neuronal interactions through neuronal synchronization. *Science* 316(5831):1609–1612.
13. Gieselmann MA, Thiele A (2008) Comparison of spatial integration and surround suppression characteristics in spiking activity and the local field potential in macaque V1. *Eur J Neurosci* 28(3):447–459.
14. Bastos AM, et al. (2012) Canonical microcircuits for predictive coding. *Neuron* 76(4): 695–711.
15. Schoffelen JM, Oostenveld R, Fries P (2005) Neuronal coherence as a mechanism of effective corticospinal interaction. *Science* 308(5718):111–113.
16. Schoffelen JM, Poort J, Oostenveld R, Fries P (2011) Selective movement preparation is subserved by selective increases in corticomuscular gamma-band coherence. *J Neurosci* 31(18):6750–6758.
17. Ray S, Maunsell JH (2010) Differences in gamma frequencies across visual cortex restrict their possible use in computation. *Neuron* 67(5):885–896.
18. Vinck M, van Wingerden M, Womelsdorf T, Fries P, Pennartz CM (2010) The pairwise phase consistency: A bias-free measure of rhythmic neuronal synchronization. *Neuroimage* 51(1):112–122.
19. Vinck M, Battaglia FP, Womelsdorf T, Pennartz C (2012) Improved measures of phase-coupling between spikes and the Local Field Potential. *J Comput Neurosci* 33(1): 53–75.
20. Fries P, Womelsdorf T, Oostenveld R, Desimone R (2008) The effects of visual stimulation and selective visual attention on rhythmic neuronal synchronization in macaque area V4. *J Neurosci* 28(18):4823–4835.
21. Fries P, Roelfsema PR, Engel AK, König P, Singer W (1997) Synchronization of oscillatory responses in visual cortex correlates with perception in interocular rivalry. *Proc Natl Acad Sci USA* 94(23):12699–12704.
22. Sobotka S, Ringo JL (1994) Stimulus specific adaptation in excited but not in inhibited cells in inferotemporal cortex of macaque. *Brain Res* 646(1):95–99.
23. Li L, Miller EK, Desimone R (1993) The representation of stimulus familiarity in anterior inferior temporal cortex. *J Neurophysiol* 69(6):1918–1929.
24. Miller EK, Li L, Desimone R (1993) Activity of neurons in anterior inferior temporal cortex during a short-term memory task. *J Neurosci* 13(4):1460–1478.
25. Mitchell JF, Sundberg KA, Reynolds JH (2007) Differential attention-dependent response modulation across cell classes in macaque visual area V4. *Neuron* 55(1): 131–141.
26. Vinck M, Womelsdorf T, Buffalo EA, Desimone R, Fries P (2013) Attentional modulation of cell-class-specific gamma-band synchronization in awake monkey area v4. *Neuron* 80(4):1077–1089.
27. Womelsdorf T, et al. (2012) Orientation selectivity and noise correlation in awake monkey area V1 are modulated by the gamma cycle. *Proc Natl Acad Sci USA* 109(11): 4302–4307.
28. van Wingerden M, Vinck M, Lankelma JV, Pennartz CM (2010) Learning-associated gamma-band phase-locking of action-outcome selective neurons in orbitofrontal cortex. *J Neurosci* 30(30):10025–10038.
29. van Wingerden M, et al. (2012) NMDA receptors control cue-outcome selectivity and plasticity of orbitofrontal firing patterns during associative stimulus-reward learning. *Neuron* 76(4):813–825.
30. Stopfer M, Laurent G (1999) Short-term memory in olfactory network dynamics. *Nature* 402(6762):664–668.
31. Ringo JL (1996) Stimulus specific adaptation in inferior temporal and medial temporal cortex of the monkey. *Behav Brain Res* 76(1-2):191–197.
32. Wang Y, Iliescu BF, Ma J, Josić K, Dragoi V (2011) Adaptive changes in neuronal synchronization in macaque V4. *J Neurosci* 31(37):13204–13213.
33. Kaliukhovich DA, Vogels R (2012) Stimulus repetition affects both strength and synchrony of macaque inferior temporal cortical activity. *J Neurophysiol* 107(12): 3509–3527.
34. Huber R, et al. (2013) Human cortical excitability increases with time awake. *Cereb Cortex* 23(2):332–338.
35. Vinck M, et al. (2010) Gamma-phase shifting in awake monkey visual cortex. *J Neurosci* 30(4):1250–1257.
36. Friese U, Supp GG, Hipp JF, Engel AK, Gruber T (2012) Oscillatory MEG gamma band activity dissociates perceptual and conceptual aspects of visual object processing: A combined repetition/conceptual priming study. *Neuroimage* 59(1):861–871.
37. Buzsáki G, Wang XJ (2012) Mechanisms of gamma oscillations. *Annu Rev Neurosci* 35: 203–225.
38. Reynolds JH, Chelazzi L, Desimone R (1999) Competitive mechanisms subserve attention in macaque areas V2 and V4. *J Neurosci* 19(5):1736–1753.
39. Brunet N, et al. (2013) Visual cortical gamma-band activity during free viewing of natural images. *Cereb Cortex*, 10.1093/cercor/bht280.
40. Rubehn B, Bosman C, Oostenveld R, Fries P, Stieglitz T (2009) A MEMS-based flexible multichannel ECoG-electrode array. *J Neural Eng* 6(3):036003.
41. Fries P, Reynolds JH, Rorie AE, Desimone R (2001) Modulation of oscillatory neuronal synchronization by selective visual attention. *Science* 291(5508):1560–1563.

Supporting Information

Brunet et al. 10.1073/pnas.1309714111

SI Discussion

Two previous studies investigated gamma-band activity in rat orbitofrontal cortex during an olfactory learning task (1, 2). When rats performed the task roughly 20 times, with corresponding repeated odor presentations, orbitofrontal gamma-band activity increased steadily. Across animals and sessions, the rate of gamma increase was correlated with the rate of behavioral learning. This increase might be the vertebrate equivalent of an increase in 20 ± 5-Hz activity found in the insect olfactory system, specifically locust antennal lobe projection neurons, over the course of about 10 odor presentations (3). These observations with olfactory stimuli might be related to the results described here, although this is difficult to judge, given the different species, brain areas, and sensory systems involved.

Numerous papers have reported repetition suppression (i.e., a reduced neuronal firing rate response to the repeated presentation of a given visual stimulus) (4–8). Repetition suppression has primarily been reported for neurons in inferotemporal cortex activated with images of objects and mostly for a few presentations separated by a few intervening stimuli. In contrast, we investigated early and intermediate visual cortex and used numerous presentations. Nevertheless, the monotonic decrease in area V4 multiunit firing rates with the repeated grating presentation (Fig. 4*D*) is at least similar to the decrease in the firing rates of inferior temporal cortex neurons for roughly 10 presentations of a given object image interspersed in 200 trials with other stimuli (9).

Repetition suppression has also been reported for the visually induced gamma-band response in magnetoencephalography (MEG) (10). Human subjects were shown line drawings of everyday objects or corresponding words, with each object or word repeated once, separated by two to three intervening stimuli. MEG power in the gamma-frequency band was reduced during a repeated presentation compared with the first presentation of a given object. These results appear to be in contradiction to the results reported here. There are several important differences between the studies, however, which can most likely explain the different results. First, the previous study used MEG and analyzed spectral power for several sensor clusters and several estimated sources. In contrast, we investigated electrocorticographic (ECoG) recordings from areas V1 and V4, as well as spike and local field potential (LFP) recordings from area V4. Second, the previous study repeated stimuli only once, whereas we repeated them several hundred times. Third, the previous study involved a task that required subjects to report for each stimulus whether the respective objects were man-made or of natural origin. In contrast, the monkeys in our study performed a change detection task either on one of the grating stimuli or on the fixation point.

There are a few previous studies that investigated spectral power in awake monkey visual cortex with regard to stimulus repetition. Dragoi and coworkers (11, 12) report that gamma-band activity in macaque areas V1 and V4 induced by a grating is higher when it was preceded by another grating than when it was preceded by random dots. Kaliukhovich and Vogels (13) studied multiunit activity (MUA) and LFP in inferotemporal cortex and, upon stimulus repetition, report a decrease in spectral power above 60 Hz, whereas they ascribe an observed increase at lower frequencies to a delayed decrease in power. It is hard to compare those results with our own results because (*i*) the studies of Dragoi and coworkers (11, 12) critically entail the comparison between different adaptor stimuli (i.e., gratings vs. random dot stimuli), and (*ii*) for all three studies, stimulus repetition occurred within a single trial, much more rapidly than in our study, using either two 0.3-s grating presentations separated by a 0.1-s blank period (11, 12) or two images presented for 0.5 s with an interval of 0.5 s (13).

It has been demonstrated that the time spent awake leads to a gradual build-up of cortical excitability (14, 15), which is homeostatically down-regulated again during rest or sleep. It is conceivable that the effects described here are related and represent essentially a laboratory version of the effects of prolonged wakefulness. In each recording session, visual cortical neurons were repeatedly activated, and this activation induced local and long-range gamma-band synchronization among the recording sessions. Gamma-band synchronization might be involved in synaptic plasticity (16), and the repeated stimulation might have induced a net increase in synaptic strength of the visually activated neurons. Such an increase in synaptic strength would most likely lead, in turn, to an increase in gamma-band activity. Correspondingly, the gamma increase described here might be due to such synaptic potentiation and, if so, might provide a metric of it. We have preliminary evidence supporting this interpretation. A hallmark of the wakefulness-induced accumulation of excitability is its down-regulation during rest and sleep (15). We found that short breaks in task performance, putatively containing naps, resulted in reduced gamma-band activity afterward. Fig. S8 shows gamma-band activity from the visually responsive ECoG sites in monkey E1 (same analysis as in Fig. 1*F*) for a session with a break roughly 15 min in length, during which the monkey closed its eyes. The analysis shows that there was an increase in gamma-band activity before the break. After the break, there was a reset, which was then overcome in subsequent trials. Although this is only one example, it is consistent with sleep/rest-related renormalization as proposed by Tononi and coworkers (14, 15).

SI Methods

Experimental Procedures. Four male rhesus monkeys (*Macaca mulatta*) served as subjects for the experiments presented in this study.

Two monkeys were implanted with ECoG grid electrodes (17–19). They are referred to as "monkey E1" and "monkey E2." Those experiments took place at the Donders Institute for Brain, Cognition, and Behaviour. They were approved by the Ethics Committee of Radboud University Nijmegen. The ECoG grid realized 252 subdural electrodes distributed across several superficial areas as illustrated in Fig. 1*D*. Electrodes were platinum disks 1 mm in diameter, resulting in impedances around 1 kΩ. Details of the ECoG design can be found in a study by Rubehn et al. (18). The data presented here are from the same monkeys, ECoG grids, and experimental setup as those presented by Bosman et al. (17), but they are from different recording sessions using different stimuli and/or tasks (see below).

Two additional monkeys were studied by conventional methods for microelectrode recordings. They are referred to as "monkey M1" and "monkey M2." Those experiments took place at the National Institute of Mental Health in Bethesda, MD. They were approved by the National Institute of Mental Health Intramural Animal Care and Use Committee. These experiments used tungsten microelectrodes inserted through small trepanations of the skull within a recording chamber implanted over the prelunate gyrus. The data reported here were also (partly) used elsewhere (20–27), and details of the methods can be found in a study by Fries et al. (23).

Visual Stimulation and the Behavioral Paradigm. Visual stimulation and the behavioral paradigm were highly similar for the two experiments. We first describe the common aspects and then specify the differences.

Stimuli and behavior were controlled by Cortex software (National Institute of Mental Health). Stimuli were presented on a cathode ray tube monitor at 120 Hz noninterlaced. The monkey initiated a trial by touching a bar, triggering the appearance of a fixation point, and bringing its gaze into a fixation window (radius of ≤1°) around the fixation point. A trial was interrupted, and hence not rewarded, when the monkey's gaze left the fixation window or the bar was released prematurely. After a prestimulus baseline, two physically isoluminant patches of drifting grating, identical in size and eccentricity, appeared. The two gratings always had orientations that were orthogonal to each other, and they had drift directions that were incompatible with a single pattern containing both orientations and moving behind two apertures to avoid preattentive binding. On a trial-by-trial basis, the monkey was cued as to which of the two stimuli was behaviorally relevant (i.e., the target) and which one was irrelevant (i.e., the distracter). Either stimulus could change independently at an unpredictable moment in time up to several seconds after stimulus onset. Target and distracter changes were equally likely, following the same hazard rate. If the target changed and the monkey released the bar within a short time window thereafter, it was rewarded with several drops of diluted fruit juice. If the monkey released the bar in response to a distracter change, no reward, but a time-out, was given. After an ignored distracter change, the trial continued until a target change occurred. Missed target changes were followed by a time-out without reward.

Specific parameters of the experiments in monkeys E1 and E2 were as follows. The fixation windows had a radius of 0.85° in monkey E1 and a radius of 1° in monkey E2. Gratings had the following specifications: sine-wave luminance modulation of 100% contrast, diameter of 3°, spatial frequency of approximately one cycle per degree, and drift velocity of ∼1° per second. A prestimulus fixation baseline was 0.8 s long. Cueing was done as in the study by Boseman et al. (17): In any given trial, one grating was tinted yellow and the other was tinted blue, with the color assigned randomly across trials. The yellow and blue colors were physically equiluminant. At 0.8–1.5 s after stimulus onset, the fixation point changed color to match the color of one of the two gratings, thereby indicating this grating as the target and the other as the distracter. The stimulus change was a transient (0.15 s in length) bend of the grating, and it could occur up to 4.5 s after cue onset. On average, 89% of bar releases were correct reports of changes in the relevant stimulus.

Specific parameters of the experiments in monkeys M1 and M2 were as follows. The fixation windows had a radius of 0.7° in both monkeys. Gratings had the following specifications: square-wave black-and-white luminance modulation of 100% contrast, diameter of 2–3°, spatial frequency of one to two cycles per degree, and drift velocity of 1–2° per second. A prestimulus fixation baseline was 1.5 s in length. Cueing was done either symbolically with the color of the fixation point cueing attention to the upper or lower stimulus, with a small line with a length of 0.75° that was presented ∼1.5 s before stimulus onset and pointed to the location of the target, or through a block design without explicit cueing within a given trial. The stimulus change could occur up to 5 s after stimulus onset, and it consisted of a change of the white grating stripes into isoluminant yellow, which remained yellow for the rest of the trial. On average, 85% of bar releases were correct reports of changes in the relevant stimulus.

Our analysis did not reveal any consistent differences in the increase between the attention conditions (Fig. S4); therefore, trials from the different attention conditions were pooled for the analysis presented here.

To test whether the observed increase depended on attention being generally directed to the stimulus that induced the gamma-band synchronization, we also recorded data in a control task in monkey E1. During the control recordings, the monkey reported a color change of the fixation point while a single task-irrelevant sine-wave drifting grating was shown. The grating covered the lower right visual quadrant (contralateral to the ECoG) out to an eccentricity of roughly 10–15°.

Data Analysis. Analyses were done in MATLAB (MathWorks), using the FieldTrip open source MATLAB toolbox (http://fieldtrip.fcdonders.nl) (28).

Specific parameters for the analysis of the ECoG data were as follows. In the ECoG data, the stimuli were presented first, followed by the attentional cue. To focus on the period of sustained visual activation and attention, we used from each correctly completed trial the data from 0.3 s after cue onset until the first change in one of the grating stimuli. These data were cut into nonoverlapping epochs with a length of 0.5 s, discarding remaining data at the end. From the prestimulus baseline periods, we obtained 0.5-s epochs end-aligned to 30 ms before stimulus onset. Subsequently, we calculated local bipolar derivatives (i.e., differences determined on a sample-by-sample basis in the time domain) between LFPs from immediately neighboring electrodes to remove the common recording reference. We refer to the bipolar derivatives as "sites." Next, per site and individual epoch, the mean was subtracted. Finally, these differentiated, mean-subtracted 0.5-s epochs were Hanning-tapered and Fourier-transformed to estimate power and coherence spectra from 2 to 130 Hz, in steps of 2 Hz. The gamma band was defined as 52–74 Hz in monkey E1 and 68–82 Hz in monkey E2. Stimulus sensitivity per site was quantified by a paired t test on gamma-band power across trials between baseline and stimulation epochs. The center of mass of the gamma-band power (coherence; Fig. S6) was determined as follows. The frequencies in the gamma band were multiplied by the corresponding power (coherence) values; these products were then summed and divided by the sum of the power (coherence) values.

Specific parameters for the analysis of the microelectrode data were as follows. In the microelectrode data, the cue was presented first and the stimuli, or a block design, were then used without explicit cueing within the trial. In any case, there was at least a 1-s period of clean baseline between cue onset plus 0.3 s and the onset of the stimuli. To focus on the period of sustained visual activation and attention, we used from each correctly completed trial the data from 0.3 s after stimulus onset until the first change in one of the grating stimuli. These data were cut into nonoverlapping epochs of 0.5 s in length, discarding remaining data at the end. From the prestimulus baseline periods, we obtained two nonoverlapping 0.5-s epochs end-aligned to stimulus onset. Offline spike sorting was performed using principal component analysis (Offline Sorter; Plexon). We used the following criteria to include a single unit in our sample: It had to be well isolated from the MUA on at least one of the first two principal component analysis scores of the waveforms, its isolation had to be stable across time, and a clear refractory period had to be visible in the interspike interval distribution.

Phase-locking analysis was carried out using the methods described by Vinck et al. (29). For each neuron separately, we computed a measure of spike-LFP phase consistency called the pairwise phase consistency (PPC). For each spike of a given neuron and each frequency (f), we computed the phase of spiking relative to a given LFP channel by cutting out an LFP segment with a length of $5/f$ second, multiplying it by a Kaiser taper window (beta = 9), and then computing the discrete Fourier transform of the tapered LFP signal. We then computed, for each spike separately, the circular mean phase across all of the LFP channels, where we ignored the LFP from the electrode on which the unit was recorded. This yielded, for a given neuron, one spike-LFP phase

value per spike. For the ith spike in the kth trial, we denote the real-valued average spike-LFP phase as $\theta_{k,i}(f)$. A standard measure of spike-LFP phase locking now equals the resultant length, R, of spike-LFP phases across all selected spikes. This measure is strongly biased by the number of spikes, however (30). Similar to several recent studies (2, 31–33), we therefore computed an unbiased estimator of spike-LFP phase locking called PPC, defined as

$$\mathrm{PPC} = \frac{\sum_{k=1}^{K}\sum_{m\neq k}^{K}\sum_{i=1}^{N_k}\sum_{j=1}^{N_m}\cos\left(\theta_{k,i}(f)-\theta_{m,j}(f)\right)}{\sum_{k=1}^{K}\sum_{m\neq k}^{K}N_m N_k}.$$

Here, K is the number of trials, and N_m and N_k are the numbers of spikes in trials m and k, respectively. The PPC estimator considers one pair of spike-LFP phases, $\theta_{k,i}(f)$ and $\theta_{m,j}(f)$, from two separate trials k and m at a time. For each such pair of spike-LFP phases, it then computes the phase relation using the inner product $\cos(\theta_{k,i}(f) - \theta_{m,j}(f))$, where a value of 1 indicates that the two spike-LFP phases were equal and a value of −1 indicates that the two spike-LFP phases were rotated 180° with respect to each other. The PPC estimator then computes the average coincidence across all pairs of spike-LFP phases from disjoint trials (k,m). The pairwise estimation procedure renders the expected value of the estimator invariant to the number of spikes. The restriction that for each pair of phases compared, the spikes should have occurred in two disjoint trials renders the estimator invariant to history effects within spike trains, such as bursting and refractoriness. This is important because these history effects can cause statistical dependencies between spike-LFP phases, which can bias the PPC measure (29). Vinck et al. (29) have shown that the expected value of the PPC equals the squared resultant length $R^2 = |\mathrm{E}[\exp(i\theta)]|^2$, where θ is a random circular variable that is identically distributed to $\theta(m,j)$ for all (m,j). Once the PPC values were computed separately for each neuron, the mean and SEM were computed across neurons. A neuron was only used if there were at least 50 spikes for each spike-LFP PPC computation involving that neuron (i.e., if each trial-number bin contained at least 50 spikes), similar to previous applications of the PPC metric (1, 2, 30–32).

1. van Wingerden M, Vinck M, Lankelma JV, Pennartz CM (2010) Learning-associated gamma-band phase-locking of action-outcome selective neurons in orbitofrontal cortex. *J Neurosci* 30(30):10025–10038.
2. van Wingerden M, et al. (2012) NMDA receptors control cue-outcome selectivity and plasticity of orbitofrontal firing patterns during associative stimulus-reward learning. *Neuron* 76(4):813–825.
3. Stopfer M, Laurent G (1999) Short-term memory in olfactory network dynamics. *Nature* 402(6762):664–668.
4. Sobotka S, Ringo JL (1994) Stimulus specific adaptation in excited but not in inhibited cells in inferotemporal cortex of macaque. *Brain Res* 646(1):95–99.
5. Ringo JL (1996) Stimulus specific adaptation in inferior temporal and medial temporal cortex of the monkey. *Behav Brain Res* 76(1-2):191–197.
6. Grill-Spector K, Malach R (2001) fMR-adaptation: A tool for studying the functional properties of human cortical neurons. *Acta Psychol (Amst)* 107(1-3):293–321.
7. Miller EK, Li L, Desimone R (1993) Activity of neurons in anterior inferior temporal cortex during a short-term memory task. *J Neurosci* 13(4):1460–1478.
8. Desimone R (1996) Neural mechanisms for visual memory and their role in attention. *Proc Natl Acad Sci USA* 93(24):13494–13499.
9. Li L, Miller EK, Desimone R (1993) The representation of stimulus familiarity in anterior inferior temporal cortex. *J Neurophysiol* 69(6):1918–1929.
10. Friese U, Supp GG, Hipp JF, Engel AK, Gruber T (2012) Oscillatory MEG gamma band activity dissociates perceptual and conceptual aspects of visual object processing: A combined repetition/conceptual priming study. *Neuroimage* 59(1):861–871.
11. Hansen BJ, Dragoi V (2011) Adaptation-induced synchronization in laminar cortical circuits. *Proc Natl Acad Sci USA* 108(26):10720–10725.
12. Wang Y, Iliescu BF, Ma J, Josić K, Dragoi V (2011) Adaptive changes in neuronal synchronization in macaque V4. *J Neurosci* 31(37):13204–13213.
13. Kaliukhovich DA, Vogels R (2012) Stimulus repetition affects both strength and synchrony of macaque inferior temporal cortical activity. *J Neurophysiol* 107(12): 3509–3527.
14. Huber R, et al. (2013) Human cortical excitability increases with time awake. *Cereb Cortex* 23(2):332–338.
15. Vyazovskiy VV, Cirelli C, Pfister-Genskow M, Faraguna U, Tononi G (2008) Molecular and electrophysiological evidence for net synaptic potentiation in wake and depression in sleep. *Nat Neurosci* 11(2):200–208.
16. Vinck M, et al. (2010) Gamma-phase shifting in awake monkey visual cortex. *J Neurosci* 30(4):1250–1257.
17. Bosman CA, et al. (2012) Attentional stimulus selection through selective synchronization between monkey visual areas. *Neuron* 75(5):875–888.
18. Rubehn B, Bosman C, Oostenveld R, Fries P, Stieglitz T (2009) A MEMS-based flexible multichannel ECoG-electrode array. *J Neural Eng* 6(3):036003.
19. Brunet N, et al. (2013) Visual Cortical Gamma-Band Activity During Free Viewing of Natural Images. *Cereb Cortex*, 10.1093/cercor/bht280.
20. Fries P, Reynolds JH, Rorie AE, Desimone R (2001) Modulation of oscillatory neuronal synchronization by selective visual attention. *Science* 291(5508):1560–1563.
21. Womelsdorf T, Fries P, Mitra PP, Desimone R (2006) Gamma-band synchronization in visual cortex predicts speed of change detection. *Nature* 439(7077):733–736.
22. Womelsdorf T, et al. (2007) Modulation of neuronal interactions through neuronal synchronization. *Science* 316(5831):1609–1612.
23. Fries P, Womelsdorf T, Oostenveld R, Desimone R (2008) The effects of visual stimulation and selective visual attention on rhythmic neuronal synchronization in macaque area V4. *J Neurosci* 28(18):4823–4835.
24. Bosman CA, Womelsdorf T, Desimone R, Fries P (2009) A microsaccadic rhythm modulates gamma-band synchronization and behavior. *J Neurosci* 29(30):9471–9480.
25. Buffalo EA, Fries P, Landman R, Liang H, Desimone R (2010) A backward progression of attentional effects in the ventral stream. *Proc Natl Acad Sci USA* 107(1):361–365.
26. Buffalo EA, Fries P, Landman R, Buschman TJ, Desimone R (2011) Laminar differences in gamma and alpha coherence in the ventral stream. *Proc Natl Acad Sci USA* 108(27): 11262–11267.
27. Maris E, Womelsdorf T, Desimone R, Fries P (2013) Rhythmic neuronal synchronization in visual cortex entails spatial phase relation diversity that is modulated by stimulation and attention. *Neuroimage* 74:99–116.
28. Oostenveld R, Fries P, Maris E, Schoffelen JM (2011) FieldTrip: Open source software for advanced analysis of MEG, EEG, and invasive electrophysiological data. *Comput Intell Neurosci* 2011:156869.
29. Vinck M, Battaglia FP, Womelsdorf T, Pennartz C (2012) Improved measures of phase-coupling between spikes and the Local Field Potential. *J Comput Neurosci* 33(1):53–75.
30. Vinck M, van Wingerden M, Womelsdorf T, Fries P, Pennartz CM (2010) The pairwise phase consistency: A bias-free measure of rhythmic neuronal synchronization. *Neuroimage* 51(1):112–122.
31. Vinck M, Womelsdorf T, Buffalo EA, Desimone R, Fries P (2013) Attentional modulation of cell-class-specific gamma-band synchronization in awake monkey area v4. *Neuron* 80(4):1077–1089.
32. Womelsdorf T, et al. (2012) Orientation selectivity and noise correlation in awake monkey area V1 are modulated by the gamma cycle. *Proc Natl Acad Sci USA* 109(11): 4302–4307.
33. Parnaudeau S, et al. (2013) Inhibition of mediodorsal thalamus disrupts thalamofrontal connectivity and cognition. *Neuron* 77(6):1151–1162.

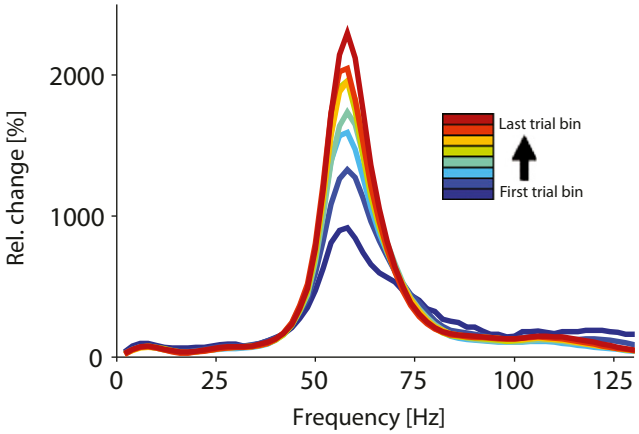

Fig. S1. Same as in Fig. 1*B* (*Inset*), but averaged over all sites with significant visually driven gamma-band activity and averaged over three sessions.

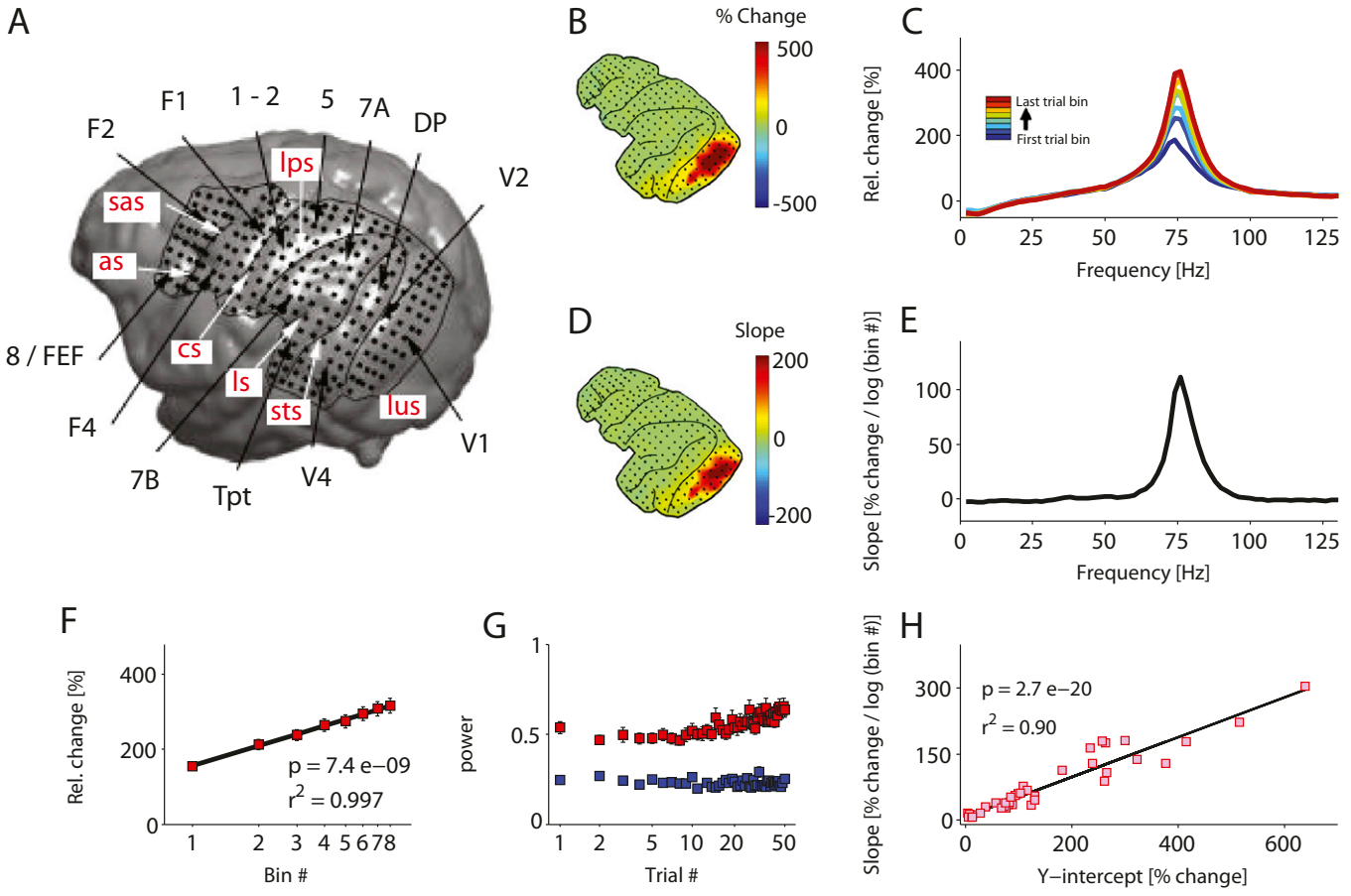

Fig. S2. *A–H* show the same analysis as Fig. 1 *D–K*, but for monkey E2.

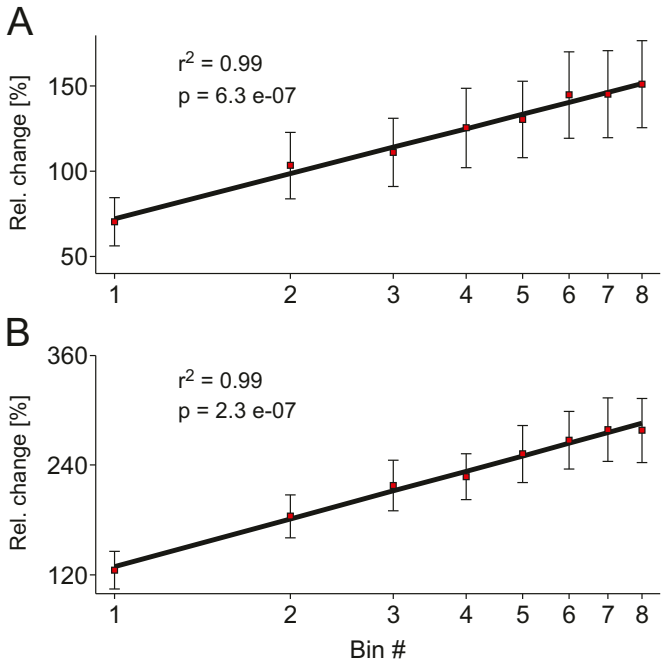

Fig. S3. (*A*) Same as in Fig. 1*I*, but for the time period 0.3–0.8 s after stimulus onset and before attentional cue onset. (*B*) Same as in *A*, but for monkey E2.

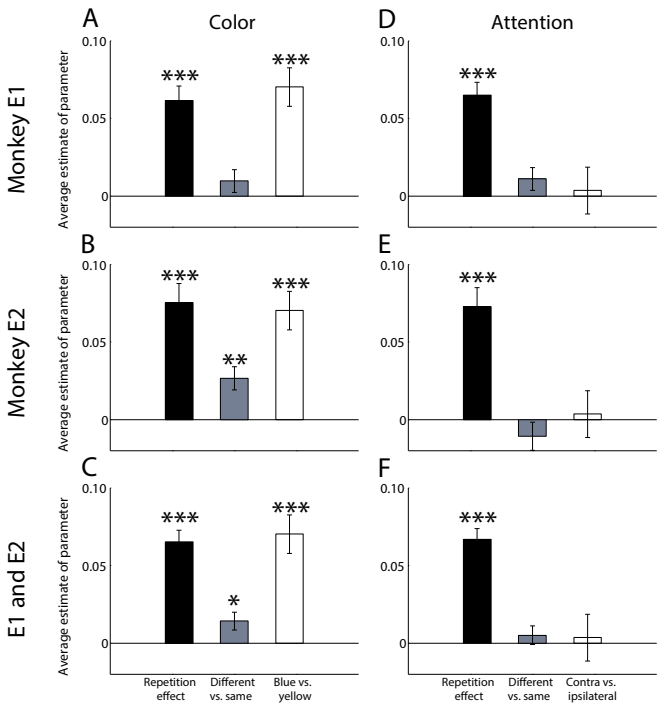

Fig. S4. Analysis testing whether the repetition-related increase of gamma-band power in area V1 was modulated by switches in stimulus features or attention. Due to the color-based trial-by-trial cueing in monkeys E1 and E2, the grating inside the receptive field was tinted blue or yellow in randomly selected trials, and orthogonally to this, it was attended or unattended in randomly selected trials. (*A–C*) To investigate whether repetition-related gamma-power increases were modulated by aspects of stimulus color, we modeled the ratio in gamma power between successive trials by a general linear model with the factors REPETITION (same in each trial to capture the general repetition effect), SWITCH (different color in two successive trials vs. same color), and COLOR (blue vs. yellow tint). The black bar confirms the repetition effect, the gray bar shows that gamma increases between trials were larger when the grating was repeated in a different color rather than the same color, and the white bar reveals that blue-tinted gratings induced stronger gamma than yellow ones. (*D–F*) To investigate whether repetition-related gamma-power increases were modulated by aspects of selective attention, we modeled the ratio in gamma power between successive trials by a general linear model with the factors REPETITION (same in each trial to capture the general repetition effect), SWITCH (across two successive trials, attention either switched from one stimulus to the other or remained focused on one stimulus), and LOCATION (attention during the second trial was focused on the stimulus in either the contralateral (Contra) or ipsilateral hemifield). Although this analysis again confirmed the repetition effect, there were no consistent effects of SWITCH or LOCATION. The absence of a LOCATION effect (i.e., the absence of a main effect of attention) is consistent with previous studies showing a mixture of small positive, negative, or no attentional effects on gamma in area V1 (1, 2). $*P = 0.05$, $**P = 0.01$, and $***P = 0.001$.

1. Buffalo EA, Fries P, Landman R, Buschman TJ, Desimone R (2011) Laminar differences in gamma and alpha coherence in the ventral stream. *Proc Natl Acad Sci USA* 108(27):11262–11267.
2. Chalk M, et al. (2010) Attention reduces stimulus-driven gamma frequency oscillations and spike field coherence in V1. *Neuron* 66(1):114–125.

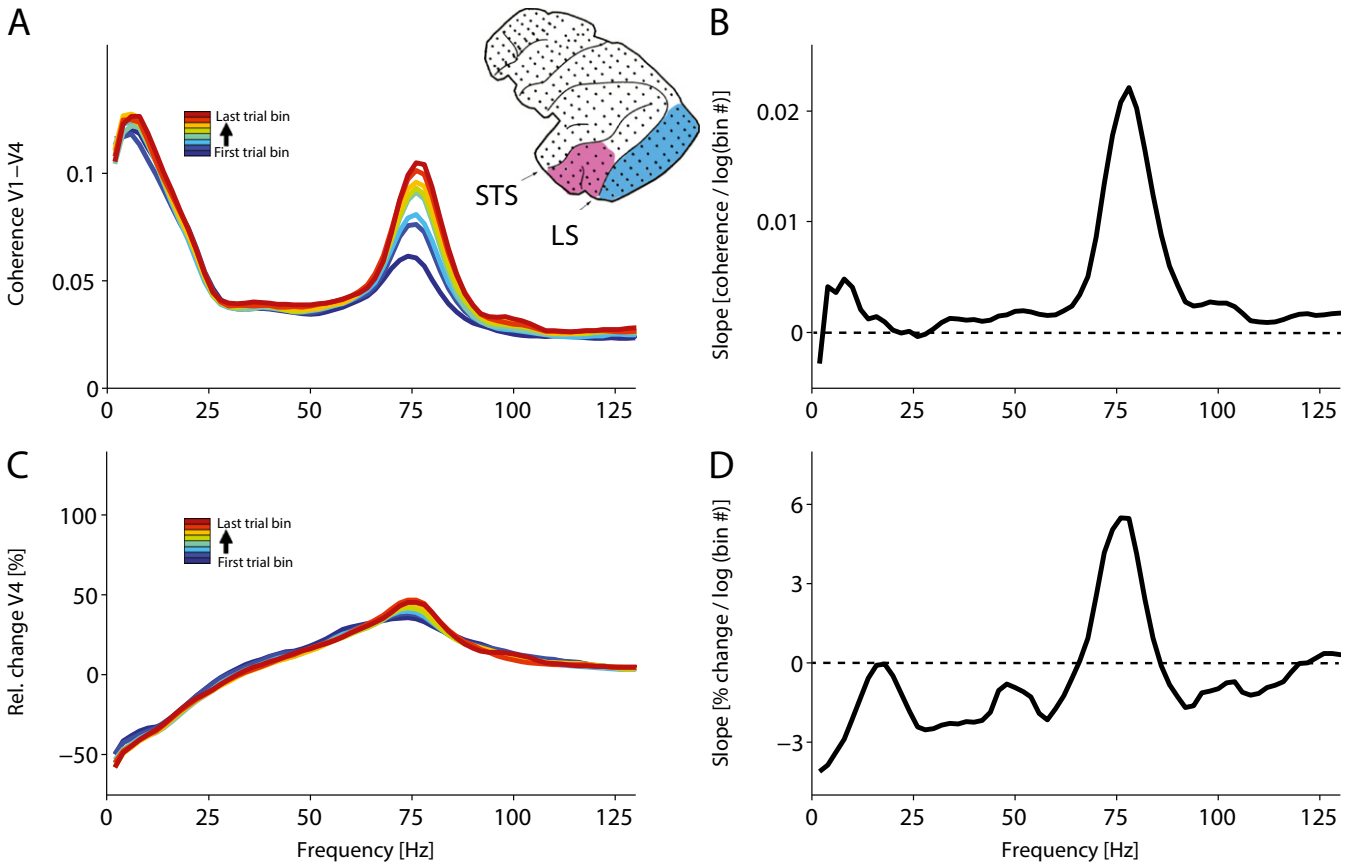

Fig. S5. *A–D* show the same analysis as Fig. 2, but for monkey E2.

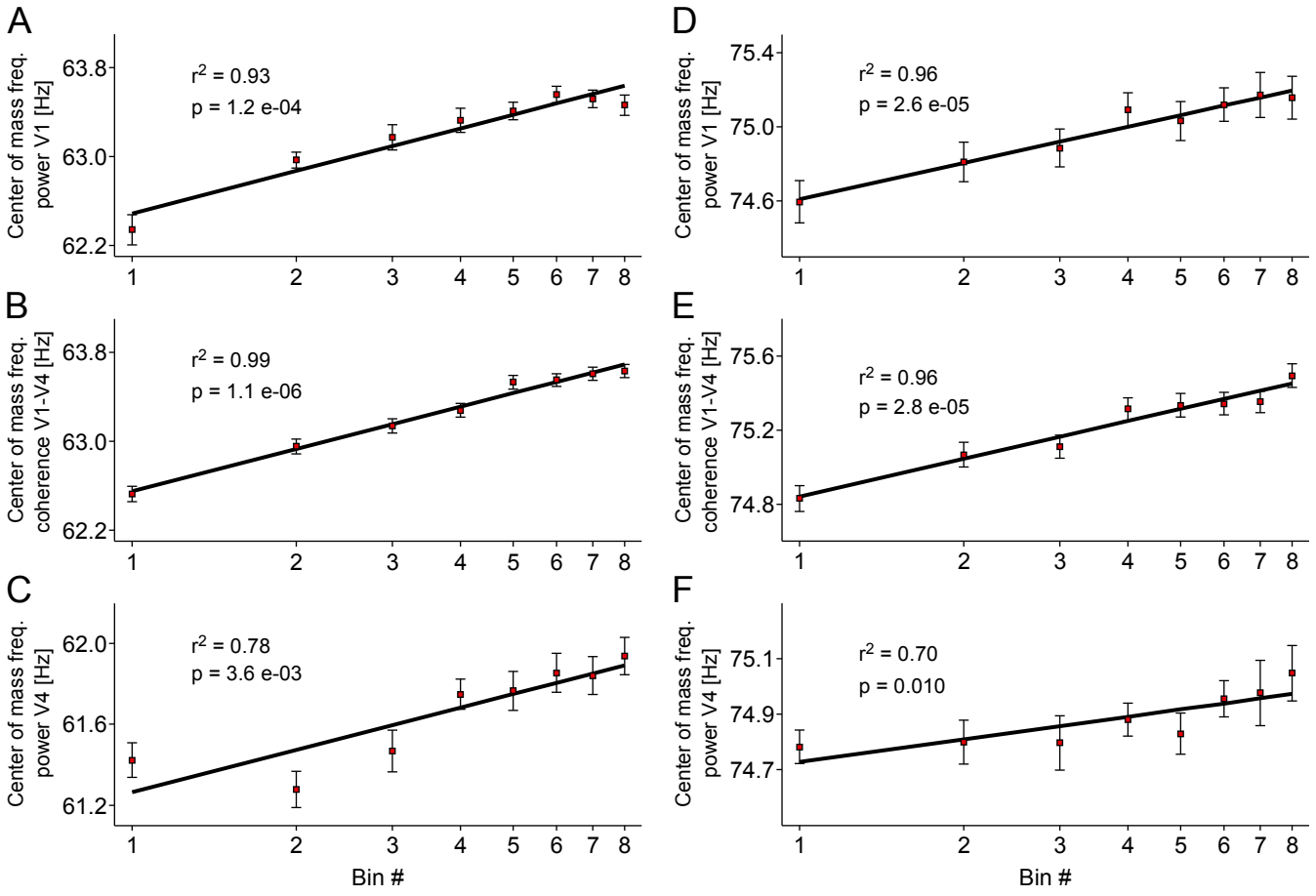

Fig. S6. Effect of stimulus repetition on the gamma frequency (freq.). (*A*) Center of mass of the visually induced gamma-band power in area V1 as a function of trial bin number on a logarithmic scale (a description of the quantification of the center of mass is provided in *SI Methods*). (*B*) Same as in *A*, but for the area V1–V4 coherence. (*C*) Same as in *A*, but for the area V4 power. (*D–F*) Same as in *A–C*, but for monkey E2.

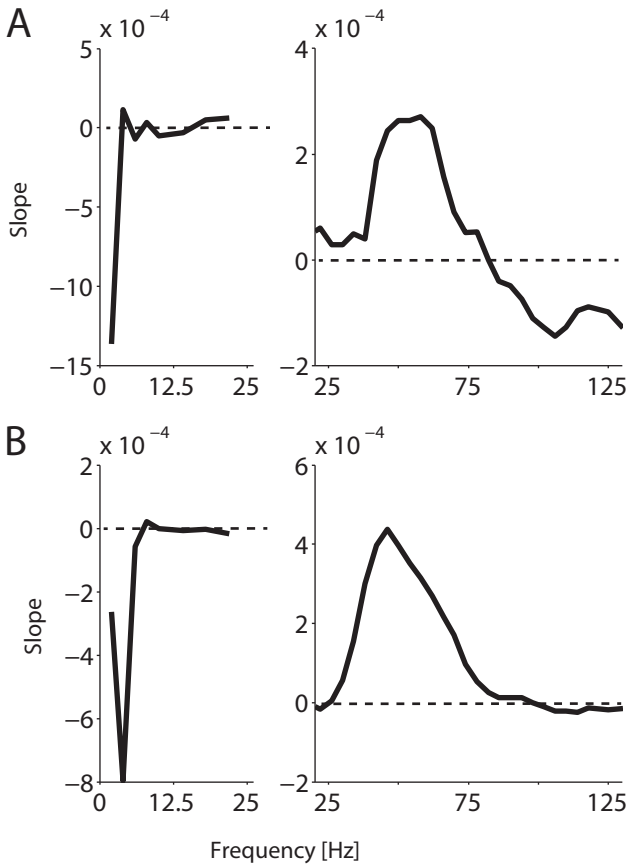

Fig. S7. Same as in Fig. 3C, but separately for monkey M1 (*A*) and monkey M2 (*B*).

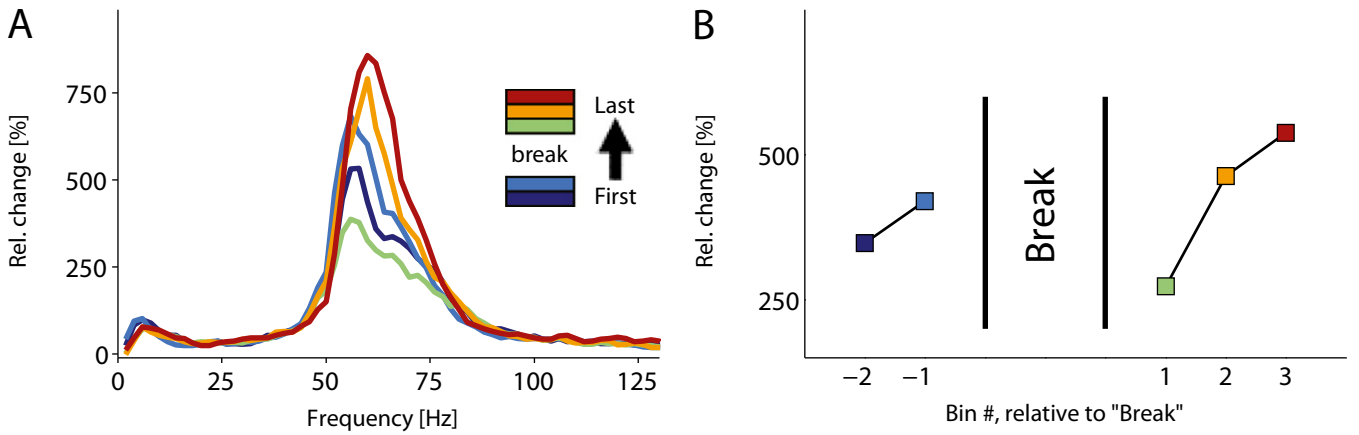

Fig. S8. Effect of a short break. (*A*) Same as in Fig. 1*F*, but during a session in which the monkey took a spontaneous break of ~15 min and with the trial bins aligned to this break, as indicated. (*B*) Same as in *A*, showing the stimulus-induced gamma power as a function of trial bin number.

Fig. S9. *A* and *B* show the same analysis as Fig. 3 *A* and *B* but at higher resolution.

Fig. S9

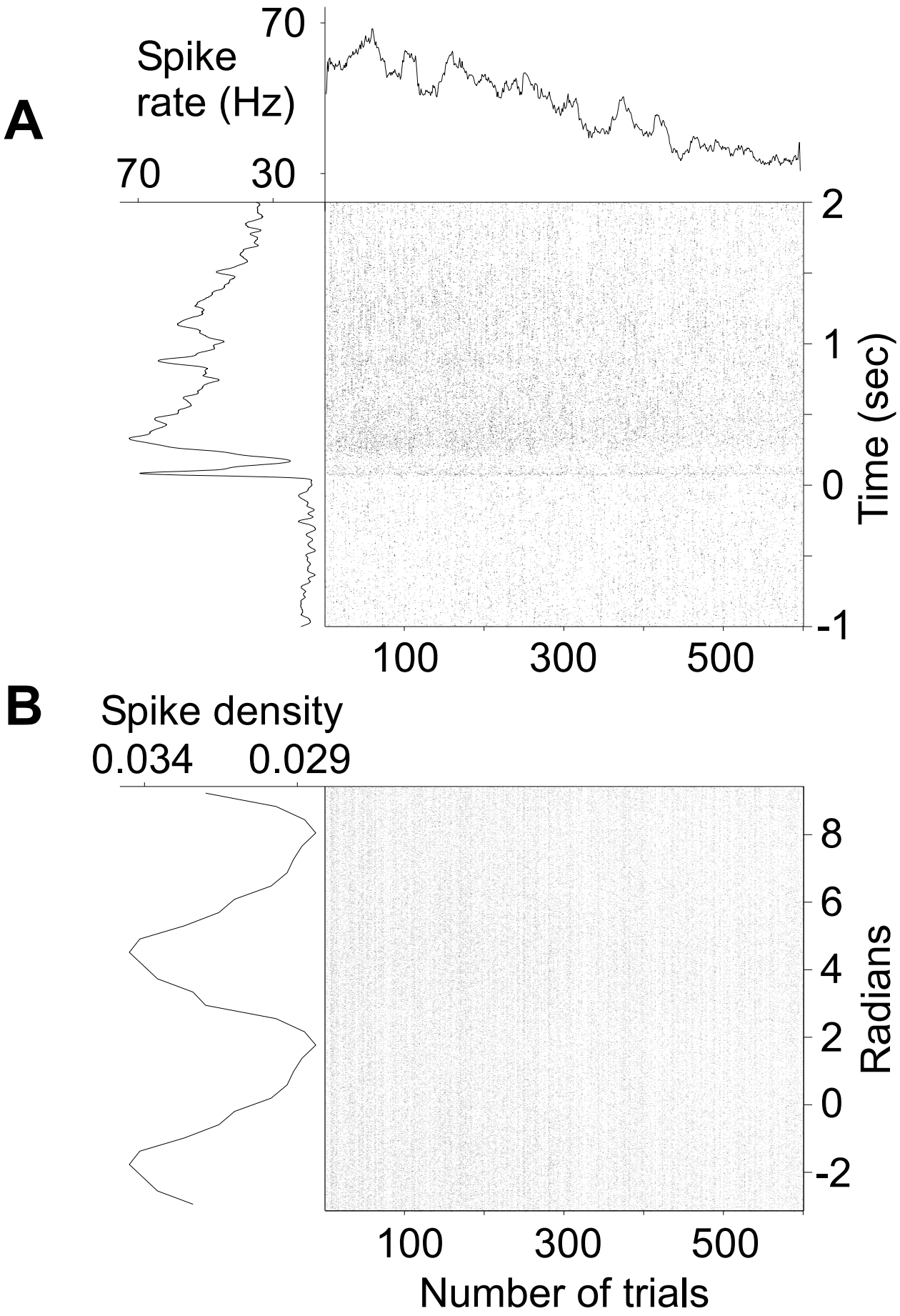

Fig. S9. *A, B* show the same analysis as Fig. 3*A, B,* but at higher resolution.